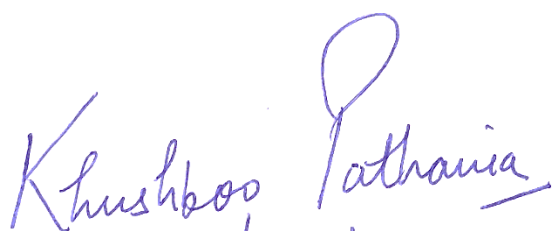


## **Details of research work**

I, hereby declare that all below mentioned details are correct to my knowledge.

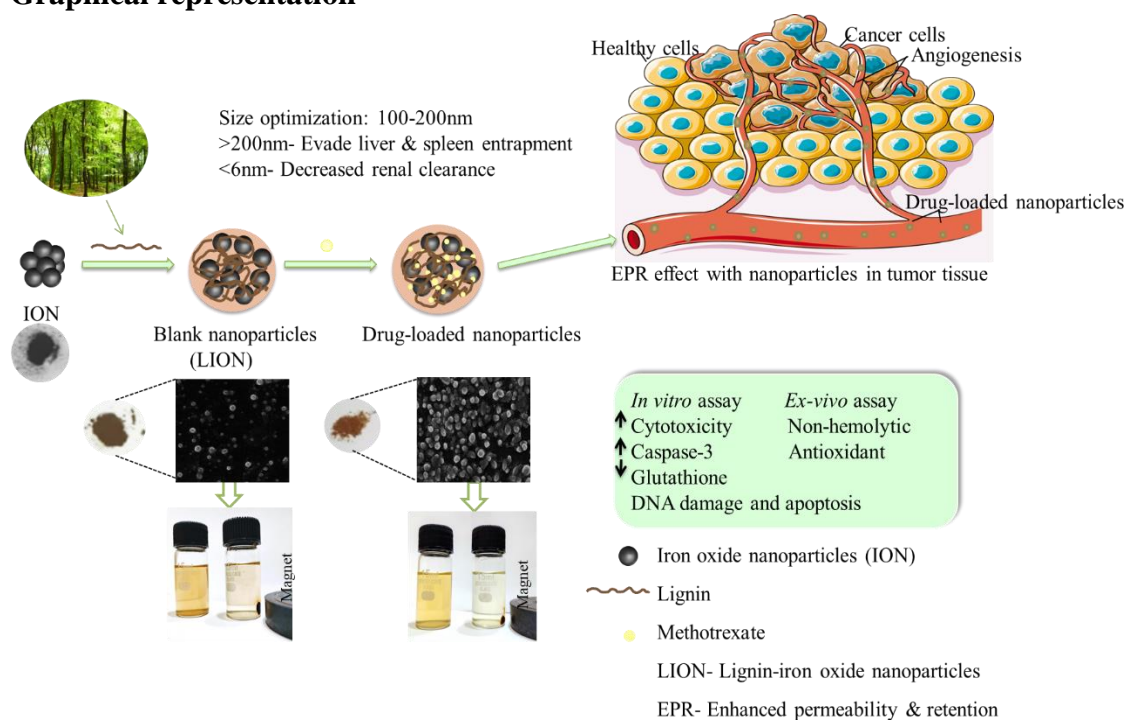
A handwritten signature in blue ink, reading "Khushboo Pathania". The signature is written in a cursive style with a large loop at the end of the last name.

**Khushboo Pathania**

## Title

Green synthesis of magnetic lignin nanoparticles as bio-carrier for therapeutics

## Graphical representation



## Introduction

Cancer afflicts nearly 20 million individuals each year<sup>1</sup>. The disease is characterized by uncontrolled cellular growth and can rapidly spread to other parts of the body if left unchecked. Although chemotherapy continues to be the first line of defense against numerous cancers, the treatment suffers from a number of limitations. Chemotherapy is poorly specific and usually causes adverse side-effects. Moreover, the drug molecules are not very soluble in biofluids and cancers eventually develop resistance to the treatment<sup>2</sup>. Nanomedicines directly address these shortcomings and can improve the stability, solubility and circulating half-life of the drug compound<sup>3</sup>. In fact, the unique pathophysiology of tumor cells and their microenvironment, including leaky vasculature and dysfunctional lymphatic drainage, play to the strengths of nanomedicines. Nanoparticles in the size range of 200-400 nm have been shown to accumulate passively at high concentrations within tumors<sup>4,5</sup> and thereafter release drugs in the vicinity of the cancer cells<sup>6</sup>. When passive targeting of tumors proves to be insufficient, nanoparticles can also be chemically modified or conjugated with targeting ligands such as antibodies to stimulate targeted delivery<sup>7</sup>. Magnetization through the inclusion of iron oxide is one of the most common approaches to actively target nanoparticles to their intended site of action, and magnetic nanoparticles have been employed as theranostic systems, drug delivery vehicles, bioimaging contrast agents and nutritional supplements for the treatment of anemia<sup>8</sup>. However, the accumulation of iron oxide within cells can catalyze the formation of reactive oxygen

species (ROS), which can elicit cytotoxic effects on account of oxidative stress<sup>9</sup>. Bare nanoparticles of iron oxide are also susceptible to aggregation and degrade rapidly *in vivo*<sup>10</sup>.

Coating magnetic iron oxide nanoparticles with a biocompatible polymer offers a compelling solution for active targeting of tumors that overcome all foreseeable limitations of bare nanoparticles. To this end, lignin is a highly promising candidate. It is abundant, non-toxic, biodegradable and cheap<sup>11</sup>, and its uniquely branched structure that is suffused with functional groups make it amenable to facile chemical modification<sup>12</sup>. In the current study, we synthesized magnetic nanoparticles of iron oxide and coated them using lignin. We subsequently conjugated the coated particles to methotrexate (MTX), an anti-metabolite drug that elicits anti-cancer activity through antagonism of folic acid metabolism. Like most potent chemotherapeutic agents, MTX is poorly soluble in water, distributes non-specifically, adsorbs variably in tissues, has a short circulation half-life, is nephro- and hepatotoxic and loses efficacy over time owing to development of resistance<sup>13</sup>. Our synthetic scheme achieves a lignin-to-drug ratio of 1:3, and drug loading and encapsulation efficiencies of 66.0% and 64.9%, respectively. Moreover, the nanoparticles retain their magnetism and bear a smooth, polyhedral geometry. The particles also have a characteristic dimension of 110-130 nm, which makes them well-suited for rapid uptake into cancer cells on account of receptor-mediated endocytosis. We confirmed these conclusions in breast cancer and macrophage cellular assays. In fact, the nanoparticles are non-hemolytic and markedly less cytotoxic compared to the pure drug and they also exhibit a concentration-dependent release of MTX for the initial 24 hours, followed by slow, sustained release. The lower cytotoxicity of the particles despite higher targeting, uptake and internalization into the cells may be attributable to lignin's high anti-oxidant effect, which neutralizes the oxidative tendencies of iron oxide. On the other hand, lignin, iron oxide and, to an extent, MTX act synergistically to enhance caspase-3 activity and reduce glutathione levels in the breast cancer cells. These results confirm that not only does our novel design overcome MTX's limitations, but the system's physicochemical properties, release kinetics and biological make it a highly effective anti-cancer treatment. These conclusions, in conjunction with the fact that lignin is an excellent chassis for chemical modification, pave the way for the development of 'intelligent' lignin-based theranostic nanoprobes that are significantly more efficacious than current therapeutics.

## Objectives

1. Synthesis of iron oxide nanoparticles and preparation of lignin-iron oxide nanoparticles (LION) by various methods.
2. Physicochemical evaluation (size and stability) of the prepared lignin-iron oxide nanoparticles.
3. Encapsulation of the anticancer drug in lignin-iron oxide nanoparticles
4. Drug-loading and optimization studies.
5. In-depth physicochemical characterization of blank (lignin-coated iron oxide nanoparticles) and drug-loaded nanoparticles
6. *In-vitro* drug release and release kinetic studies.

7. *In-vitro* cell-based studies to evaluate the hemotoxicity and cytotoxicity of the prepared formulation.
8. To determine the effect of formulation on caspase-3 and glutathione activity of breast cancer cells.
9. To study the cellular uptake of the formulation in breast cancer cells.
10. To determine the effect of formulation on nuclear condensation and DNA damage on breast cancer cells.

## Material and methods

**Chemicals, reagents and cells.** Alkali lignin (AL) was purchased from Sigma-Aldrich India. Methotrexate hydrate was purchased from Tokyo Chemical Industry. Ferric chloride hexahydrate, ferrous sulfate heptahydrate and the nanoparticle dispersing agent were purchased from Thermo Fischer Scientific India. Dulbecco's Modified Eagle's Medium (DMEM), streptomycin and penicillin were purchased from Lonza. 2,2-Diphenyl-1-picryl hydrazyl (DPPH), Roswell Park Memorial Institute 1640 medium (RPMI 1640), fetal bovine serum (FBS) and phosphate-buffered saline (PBS) were purchased from HiMedia India. FITC and NP 40 lysis buffer were purchased from Invitrogen and protease inhibitor cocktail was purchased from Genetix Biotech. We obtained RAW 264.7 murine macrophage, HeLa human cervical cancer and MDA-MB-231 human breast cancer cell lines from the National Center for Cell Science (NCCS, Pune, India). The HeLa cells were cultured in RPMI 1640, whereas the RAW and breast cancer cells were maintained in DMEM. Both media were supplemented with 10% FBS and 1% penicillin-streptomycin and the cultures were incubated at 37°C in a humidified 5% CO<sub>2</sub>-95% air atmosphere.

**Synthesis of iron oxide nanoparticles.** We used chemical co-precipitation to synthesize iron oxide<sup>14</sup>. We initially dissolved ferric chloride hexahydrate and ferrous sulfate heptahydrate in deionized water to final concentrations of 0.1 M each and purged both solutions with nitrogen. We then combined the solutions in a two-necked, round-bottom flask and magnetically stirred the mixture at 60°C under nitrogen for 30 min. We then added a 10 wt.% ammonia solution to the mixing solution in a dropwise manner until the pH of the solution reached 10 while gradually raising temperature to 90°C. The solution changed from orange to black while stirring was maintained for another 2 h at 90°C. We then centrifuged the contents of the flask at 7000xg for 10 min and washed the precipitate three times with distilled water in order to remove any excess ammonia. We later collected the iron oxide nanoparticles using a strong magnet and dried them overnight at 80°C.

**Preparation of lignin-coated nanoparticles.** We prepared a solution of 0.5 mg/mL lignin and iron oxide in deionized water and 1 mg/mL MTX in DMSO and subsequently used three different approaches, namely *in situ* addition<sup>14</sup>, self-assembly using vortexing<sup>15</sup> and anti-solvent precipitation with ultrasonication<sup>16</sup>, to synthesize the lignin-coated iron oxide nanoparticles. *In situ* addition proceeded with the dropwise addition of the lignin solution to the iron oxide solution, followed by vigorous stirring for 8 h to yield the lignin-coated iron oxide nanoparticles (LIONs). In a parallel step, lignin and drug solutions were added dropwise

and simultaneously to the iron oxide solution and then stirred for 8 h to produce drug-loaded, lignin-coated nanoparticles. Since the physicochemical properties of the formulation are influenced greatly by the drug-to-polymer ratio, we varied the volumetric amounts of the drug and lignin solutions added to the iron oxide solution and evaluated the influence of this parameter on size, drug loading and encapsulation efficiency. Anti-solvent precipitation method was employed coupled with ultrasonication technique for preparation of blank and drug-loaded nanoparticles. Iron oxide solution was added to lignin solution under sonication and sonication was maintained for 1 h at room temperature to yield LIONs. Similarly, lignin and MTX solutions were added to iron oxide solution under sonication and sonication was maintained for 1 h at room temperature to yield drug-loaded nanoparticles. On the other hand, the vortexing method tries to exploit self-assembly and proceeds with the dropwise addition of iron oxide solution to the lignin solution, followed by vortexing for 30 min to produce LIONs. The drug is subsequently loaded by dropwise addition of MTX to the LION solution. We then isolated the nanoparticles by centrifuging the mixtures at 7000xg for 10 min and later washing the precipitate three times with distilled water in order to remove non-complexed, excess ingredients. We later collected the nanoparticles using a strong magnet and subsequently lyophilized. All methods yielded nanoparticles of comparable physical and chemical characteristics for similar operational parameters.

***Fluorescent labeling of the nanoparticles.*** Cellular uptake of the nanoparticles was evaluated through fluorescent labeling. The labeled-nanoparticles were prepared using anti-solvent precipitation with ultrasonication as described in previous section. We introduced 5 mg/mL solution of FITC in DMSO either individually (for blank nanoparticles) or in combination with the MTX solution (for drug-loaded nanoparticles) to the LION mixture under sonication and sonicated it for 1 h at room temperature. We repeated the centrifugation and washing steps and then collected the nanoparticles using a strong magnet. The particles were then lyophilized.

***Measurements of physical characteristics of the nanoparticles.*** We employed a Nano-ZS Zeta Sizer manufactured by Malvern Instruments to measure the particle size distribution and zeta potentials of the nanoparticles. The particles were suspended in deionized water along with a commercial dispersing agent in a polystyrene cuvette and exposed to a laser at an angle of 90°. We made three recordings and ensured that they are sufficiently apart in time. We also recorded the Fourier-transform infrared (FTIR) spectra and differential scanning calorimetry (DSC) thermograms of iron oxide, lignin, MTX, LIONs and drug-loaded nanoparticles. The FTIR spectra were recorded using a PerkinElmer Spectrum Two spectrometer, whereas we used a Waters Q20 TA calorimeter for the DSC measurements. We also performed high-resolution transmission electron microscopy (HRTEM) and field emission scanning electron microscopy (FESEM) using a JEM 2100 Plus electron microscope (JEOL) and scanning electron microscopy using a SU8010 electron microscope (Hitachi) to study the surface morphology of the nanoparticles. We also measured the pH of 1 mg/mL solution of LIONs in distilled water and also examined them under an external magnetic field.

***Assessment of the antioxidant activity of the nanoparticles.*** We measured the antioxidant activity of the nanoparticles using the DPPH assay. Briefly, DPPH forms a free radical in solution, thereby rendering the solution purple. The free radical is subsequently scavenged by hydrogen donors and forms a yellow-colored species. The greater a substance's antioxidant

property, the higher is the scavenging activity in the solution. Consequently, each assay mixture comprises 2 mL of 0.1 mM solution of DPPH in ethanol and 2 mL of the test sample. Ascorbic acid, a potent antioxidant, serves as the positive control. The assay is performed at 37°C for 30 min in test tubes and the absorbance is measured at 517 nm using UV-Vis spectrophotometer. The antioxidant properties or DPPH radical scavenging activity (RSA) of a substance are then quantified using Equation 1. RSA is a measure of the antioxidant's inhibition of the protonation of DPPH to form hydrazine.

$$RSA = \frac{(Absorbance\ of\ ascorbic\ acid) - (Absorbance\ of\ the\ sample)}{(Absorbance\ of\ ascorbic\ acid)} \times 100 \quad (1)$$

We plotted the RSA against DPPH concentrations and determined the IC<sub>50</sub> values for the nanoparticles. The IC<sub>50</sub> value denotes the concentration of nanoparticles that is needed to scavenge 50% of the DPPH radicals in solution.

**Calculation of drug loading and encapsulation efficiencies.** The drug loading capacity (DLC) is defined as the ratio of the weight of drug that is loaded into the nanoparticle to the weight of the entire nanoparticle. On the other hand, the encapsulation efficiency (EE) is defined as the ratio of the weight of drug that is loaded into the nanoparticle to the total weight of the drug that was added into assembly mixture. We estimated DLC and EE for the nanoparticles using direct as well as indirect approaches. In the direct method, synthesized nanoparticles were initially weighed, then solvated in DMSO and later sonicated to release the drug into the solvent<sup>17</sup>. We then estimated the concentration of MTX by measuring the UV-Vis absorbance of the solution at 303 nm. In the case of the indirect method, we estimated the concentration of free or unloaded drug in the supernatant that is produced after centrifugation<sup>18</sup>. We performed both sets of measurements on three different samples and reported the DLC and EE as the average of the six recordings.

**Determination of release kinetics and stability of the nanoparticles.** We introduced the drug-loaded nanoparticles into dialysis bags having an 8 kDa molecular weight cut-off. The bags were then suspended in 25mL of phosphate-buffered saline (PBS). We estimated the release kinetics at pH conditions of 6.3 and 7.4. The solutions were maintained at 37°C and gently agitated at 100 rpm. We frequently sampled the bulk PBS phase at pre-determined intervals. Sampling frequency was higher at the start of the experiment in order to accurately record the initial burst-release of the drug owing to the highly favourable chemical potential gradient at initial time points. We withdrew 2 mL at each sampling point and replaced 2 mL of fresh media to maintain the sink conditions. We estimated the concentrations of MTX in the samples by measuring the UV-Vis absorbance of the solution at 303 nm. We also adjusted the concentrations for dilution due to addition of fresh media. We subsequently analyzed the concentration-time data using the software package DD Solver. We fitted the data to numerous models, including zero-, first-order, Higuchi, Weibull and the Korsmeyer-Pappas models. The software package also estimates the rate constants and correlation coefficients for the models. Finally, we evaluated the stability of the formulation by estimating the size and drug content of the nanoparticles at 0, 6 and 12 months under storage at 4°C.

**Hematotoxicity measurements.** We evaluated the toxicity of the nanoparticles by studying their effect on red blood cells (RBCs) using a standard hemolysis assay. We collected 4 mL of whole rat blood and transferred the samples to EDTA to prevent coagulation. We then separated the RBCs from the samples by centrifugation at 1,500 rpm for 10 min at 4°C and subsequently washed the purified cells using ice-cold PBS. We repeated the washing and centrifugation steps numerous times until the cell suspension was clear. We subsequently mixed 20 µL of varying concentrations of MTX and the drug-loaded nanoparticles with 180 µL of the RBC suspension and incubated the mixtures at 37°C for 1 h under constant shaking. We also prepared negative and positive control mixtures PBS solution and 1% Triton X-100 in PBS, respectively. Following incubation, we centrifuged the samples at 1,500 rpm for 10 min at 4°C. The supernatant was collected and analyzed at 540 nm using a BioRad ELISA plate-based spectrophotometer. Hemolysis was quantified as:

$$\begin{aligned} & \% \text{ Hemolysis} \\ &= \frac{(\text{Absorbance of sample}) - (\text{Absorbance of saline mixture})}{(\text{Absorbance of Triton mixture}) - (\text{Absorbance of saline mixture})} \times 100 \quad (2) \end{aligned}$$

**Cytotoxicity measurements.** We employed the colorimetric MTT assay to assess cytotoxicity of the formulations<sup>19</sup>. Briefly, we seeded RAW 264.7 murine macrophage, HeLa human cervical cancer and MDA-MB-231 human breast cancer cells in individual wells of a 96-well culture plate containing 180 µL of each cell line's specific culture medium. We also individually added varying concentrations of MTX, LIONs and the drug-loaded nanoparticles to the wells. Control samples did not contain any drug or nanoparticles and blank samples did not contain any cells. The seeding density translated to  $5 \times 10^3$  cells in each well and the cultures were incubated at 37°C in an atmosphere comprising 5% CO<sub>2</sub>. Following 24 h of incubation, we replaced the supernatant in each well with fresh medium comprising 5 mg/mL of 3-(4,5-dimethylthiazol-2-yl)-2,5-diphenyltetrazolium bromide (MTT). The cultures were then incubated at 37°C for an additional 4 h. We subsequently measured the absorbance of each well at 595 nm. The absorbance of blank and control wells was assumed to be 0% and 100% viable, respectively, and we used this calibration curve to determine the viability of cells in all the wells. We thereafter determined the IC<sub>50</sub> values of the drug, LIONs or drug-loaded nanoparticles GraphPad Prism's in-built function by plotting the viability against concentration.

**Estimation of cellular activity.** We also quantified the glutathione levels and caspase-3 activity of treated and untreated MDA-MB-231 cells. We initially seeded the cells in a 24-well plate at a density of  $5 \times 10^6$  cells/well and treated them either with LIONs, MTX or drug-loaded nanoparticles at two concentrations (IC<sub>50</sub> values of MTX and drug-loaded nanoparticles). The cultures were incubated at 37°C in a humidified incubator supplied with 5% CO<sub>2</sub>. After 24 h had elapsed, we washed the cultures with ice-cold PBS and then treated the cultures with trypsin to detach them from the surface. We subsequently centrifuged the cell suspensions at 1,500 rpm for 10 minutes at room temperature to separate the supernatant and then lysed the cells with 10x NP-40 buffer supplemented with protease inhibitors. Glutathione (GSH) metabolism in the cells was quantified by supplying 5,5'-dithio-bis(2-nitrobenzoic acid)

(DTNB) to the lysates. DTNB reacts with GSH to produce a yellow-colored derivative 5'-thio-2-nitrobenzoic acid (TNB) that can be detected at 412 nm<sup>20</sup>. The decrease in GSH is determined using:

$$\begin{aligned} & \% \text{ decrease in GSH} \\ &= \frac{(\text{Absorbance of sample}) - (\text{Absorbance of control})}{(\text{Absorbance of control})} \times 100 \quad (3) \end{aligned}$$

Likewise, caspase-3 activity in the MDA-MB-231 lysates was determined using the GENLISA<sup>TM</sup> assay kit. The assay involves use of a biotinylated CASP3 antibody to bind caspase-3, followed by treatment using a streptavidin-horseradish peroxidase (HRP) conjugate and incubation at 37°C for 1 h. The mixtures were washed 4 times using the solution provided in the kit and the blotting substrates 3,3',5,5'-tetramethylbenzidine (TMB) A and B were later added. A second incubation at 37°C for 10 min followed suit, after which the stop solution was added to the samples. Absorbance of the samples was detected at 450 nm and the relative increase in caspase-3 activity was determined as:

$$\begin{aligned} & \% \text{ Increase in activity} \\ &= \frac{(\text{Absorbance of sample}) - (\text{Absorbance of control})}{(\text{Absorbance of control})} \times 100 \quad (4) \end{aligned}$$

**Cellular uptake of nanoparticles.** We also estimated the uptake of blank and drug-loaded nanoparticles by MDA-MB-231 cells. We seeded the cells on a coverslip in a 6-well plate at a density of  $2 \times 10^4$  cells/well and allowed the cells to attach by incubating the cultures for 24 h at 37°C in a 5% CO<sub>2</sub> atmosphere. The cells were then treated with FITC-labeled blank and drug-loaded nanoparticles and incubated for an additional 4 h. We then washed the cells three times with ice-cold PBS and later fixed the cells with 4% paraformaldehyde. The fixed cells were counterstained with a 10 µg/mL solution of Hoechst dye and washed a further three times with ice-cold PBS. The mounted cells were then investigated using a Nikon C2 laser-scanning confocal microscope (excitation and emission wavelengths of 352 and 450 nm, respectively<sup>21</sup>) to determine uptake of the nanoparticles.

**Identification of apoptosis.** We probed potential apoptosis using nuclear condensation and DNA fragmentation. To this end, we employed Hoechst 33342 staining. Untreated and treated cells (MTX, LIONs and drug-loaded nanoparticles) were incubated with a 10 µg/mL solution of Hoechst dye for 5 min, followed by visual analysis using a Nikon C2 laser-scanning confocal microscope under excitation and emission wavelengths of 352 and 450 nm, respectively.

## RESULTS AND DISCUSSION:

### Selection of synthesis technique and optimization of drug loading.

We investigated 3 different approaches to synthesize the lignin-iron oxide nanoparticles, namely *in situ* addition, self-assembly using vortexing and anti-solvent precipitation with ultrasonication. Analysis of the particle size distribution and polydispersity index (PDI) using



dynamic light scattering (DLS) revealed that anti-solvent precipitation with ultrasonication yielded the smallest and least polydisperse particles (**Table 1**).

**Table 1.** Effect of different techniques on particle size and polydispersity index (PDI)

	Average particle size (nm)	PDI
<i>In situ</i> addition	350.7±12	0.328±0.034
Self-assembly using vortexing	462.3±20	0.434±0.024
Anti-solvent precipitation with ultrasonication	153.3±3.2	0.182±0.017

Next, we deduced the optimal drug loading for the nanoparticles by varying the weight ratios of MTX and the LIONs (**Table 2**). The drug-nanoparticle ratio clearly influenced drug loading, particle size and PDI of the system. However, encapsulation efficiency did not vary. The diminishment in particle size with increasing drug loading is hypothesized to occur owing to an increase in hydrophobic interactions between the drug and aromatic groups in lignin. We selected a 1:3 LION:MTX ratio for subsequent testing in light of the ideal particle size and PDI. The 1:3 LION:MTX nanoparticles are hereinafter simply referred to as drug-loaded nanoparticles.

**Table 2.** Characterization of different LION:MTX ratios.

Weight ratio of LION:MTX	Encapsulation efficiency (%)	Drug loading (%)	Particle size (nm)	PDI
1:1	64.84±0.19	32.42±0.17	158.9±1.3	0.242±0.047
1:2	64.85±0.17	56.46±0.14	139.4±3.4	0.248±0.048
1:3	64.88±0.14	66.06±0.18	111.85±3.75	0.233±0.054

### Characterization of Nanoparticles:

**Physical properties of the nanoparticles.** We estimated the hydrodynamic diameters of the LIONs and drug-loaded nanoparticles using DLS to be 110.65±1.95 nm and 111.85±3.75 nm, respectively. The corresponding PDIs were determined to be 0.2305±0.0485 and 0.233±0.054, respectively (**Figure 2**). The size of the drug-loaded nanoparticles falls within the 20-200 nm range that has been reported to be conducive for passive targeting of tumors and longer residence times owing to slower clear-out from the kidneys, liver and spleen. Additionally, the PDI of 0.287 for the drug-loaded nanoparticles is indicative of uniform size and moderate polydispersity, which is desirable for efficient drug delivery. Nanoparticles with PDIs that exceed of 0.5 have been reported to agglomerate *in vivo*, which conspires to increase particle size and reduce magnetization, thereby negatively impacting delivery of the nanoparticles to the site of action and their uptake thereafter<sup>22</sup>.

The zeta potentials for iron oxide, LIONs and drug-loaded nanoparticles were recorded to be -11.6, -13.3 and -13.6 mV, respectively (Figure 1). The preponderance of hydrophobic interactions within the LIONs and drug-loaded nanoparticles translates to increased charge density of the nanoparticles, which, in turn, increases the stability of the dispersions due to higher electrostatic repulsion.

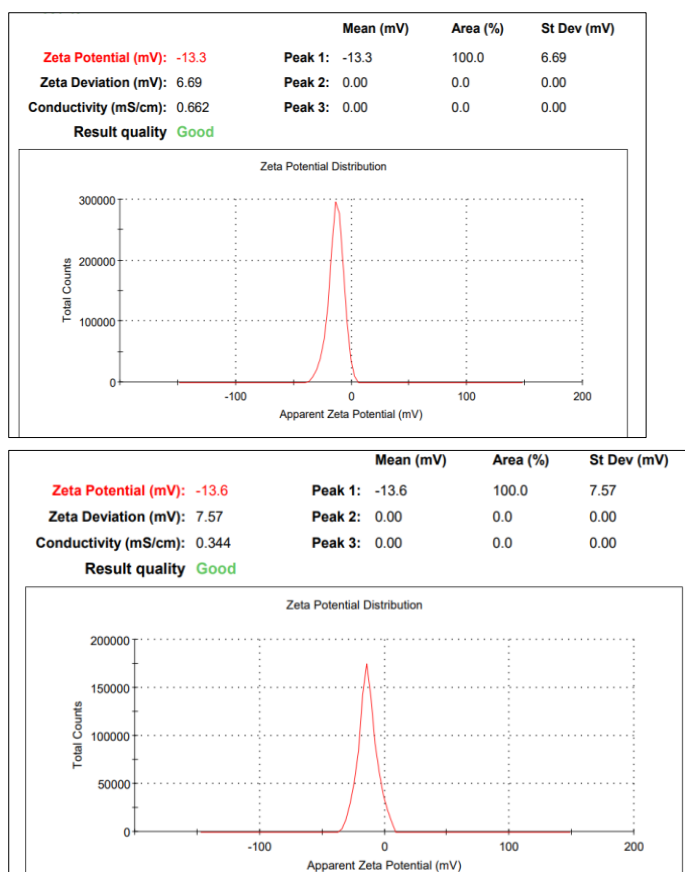


**Figure 1. Zeta potential of a. Blank nanoparticles b. Drug-loaded nanoparticles**

HRTEM micrographs reveal a polyhedral morphology for LIONs as well as drug-loaded nanoparticles, which suggests that incorporation of MTX within the LIONs does not alter their macroscopic structure (**Figure 2**). The size histogram is Gaussian and the average diameters of the LIONs and drug-loaded nanoparticles were determined to be 115.03 and 109.36 nm, respectively. These measurements are consistent with the hydrodynamic diameters measured using DLS. Additionally, LIONs exhibited pronounced aggregation compared to the drug-loaded nanoparticles. The magnetism of iron oxide is more pronounced in the former, whereas electrostatic repulsion dominates in the latter system.

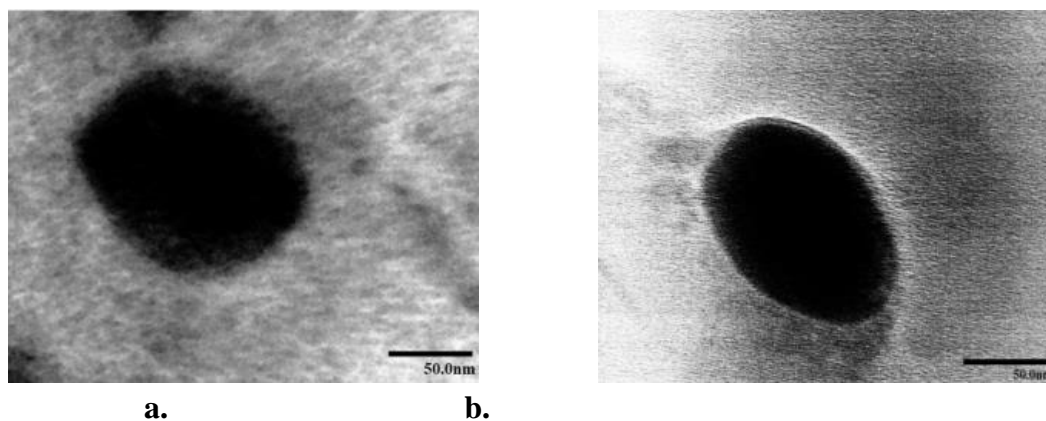


**Figure 2. HRTEM image of a. blank LION b. drug-loaded nanoparticle**

Likewise, FESEM micrographs of the LIONs revealed narrowly dispersed, smooth, spherical particle. The average diameter of the particles was estimated to be 114.3 nm. On the other hand, the drug-loaded nanoparticles showed wider distribution with majorly spherical smooth surface for single particles and a few polyhedral with rough surface for agglomerated particles (**Figure 3**). Agglomeration of particles could be attributed to the small size and high particle density due to improper dilution or drying during sample preparation. The average size was 129.19 nm which is slightly greater than that observed with DLS and HRTEM data owing to the agglomeration and thus, wider size distribution.

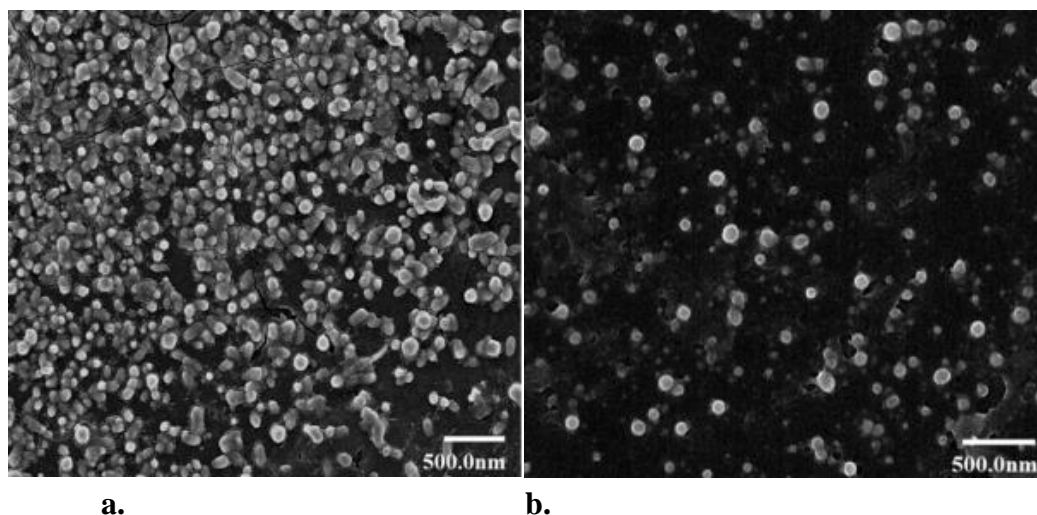


**Figure 3. FESEM image of a. blank LIONs b. drug-loaded nanoparticles**

#### **FTIR Analysis:**

FT-IR spectra of iron oxide, lignin, LION, drug, drug-loaded nanoparticles, and physical mixture (LION+Drug) (**Figure 4**) were recorded to determine the functional groups present and confirm the formation of the nanohybrids by comparing their spectra.

In Figure 7, the characteristic peak for  $\text{Fe}_3\text{O}_4$  which is absorption peaks at  $570\text{ cm}^{-1}$  belonged to the stretching vibration mode of Fe–O bonds, and  $3408\text{ cm}^{-1}$  and  $1619\text{ cm}^{-1}$  can be attributed to the stretching and bending vibrations of water adsorbed at the surface. In lignin, the bands at  $3427\text{ cm}^{-1}$  are due to O–H stretching vibration, and bands near  $3070\text{ cm}^{-1}$  are due to asymmetrical C–H stretching vibration. The peaks at  $1415$  and  $1268\text{ cm}^{-1}$  are due to the skeletal vibration and stretching vibration of the aromatic ring, absorption at  $1276\text{ cm}^{-1}$  can be attributed to C–O stretch, and  $1030\text{--}1300\text{ cm}^{-1}$  to C–C, C–O, and ether band. In the spectra of LION, the characteristic peaks of lignin and iron oxide along with more intense peaks at  $1405$  and  $1602\text{ cm}^{-1}$  can be attributed to stretching bands of carboxylate thus, confirming the successful formation of lignin-iron oxide nanoparticles.

For drug (methotrexate hydrate), characteristic absorptions band as a broad signal at  $3384\text{ cm}^{-1}$  (O–H stretching from carboxyl groups and water of crystallization), at  $3080\text{ cm}^{-1}$  (primary amine N–H stretching), at  $1645$  and  $1603\text{ cm}^{-1}$  is assigned to C=O stretching (from carboxylic and amidic groups). Bands at  $1545$  and  $1497\text{ cm}^{-1}$  correspond to N–H bending from amide overlapping with aromatic  $\text{--C=C}$  stretching and from  $1400\text{--}1200\text{ cm}^{-1}$  corresponds to  $\text{--C--O}$

stretching from carboxylic group,  $1090\text{ cm}^{-1}$  to O–H bending out of the plane, and  $830\text{ cm}^{-1}$  to C–H (2-adjacent hydrogens on an aromatic ring, para substitution) <sup>25</sup>.

The spectra of the drug-loaded nanoparticles and the physical mixture (LION+drug) when compared showed no significant difference except for an extra sharp peak at  $1720\text{ cm}^{-1}$  probably due to C=O stretching from carbonyl thus suggesting no drug-polymer interaction and thereby confirming successful drug loading.

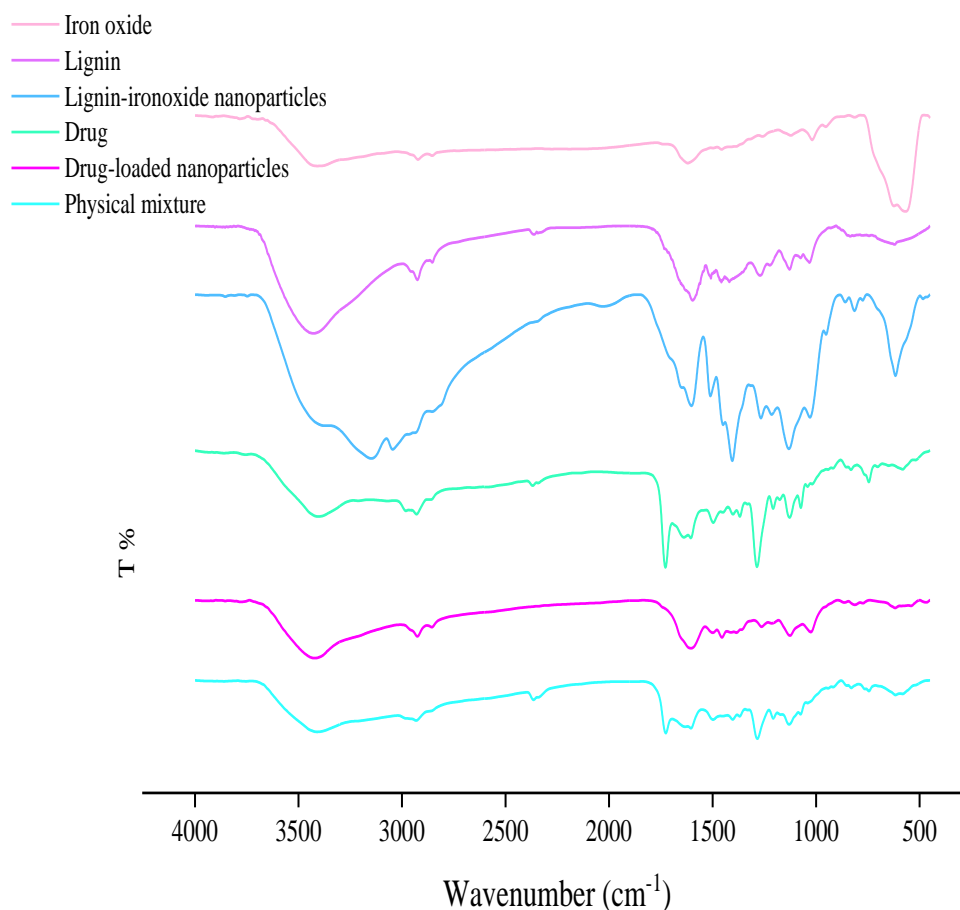


**Figure 4. FT-IR spectra of iron oxide, lignin, LION, drug, drug-loaded nanoparticles, and physical mixture**

#### DSC:

DSC thermograms were used to study the thermal peaks of the drug and polymer and their interaction in the formulation. DSC thermal curve of the formulation was compared with pure drug, blank and physical mixture (Figure 18). It was observed that the DSC thermal peak of the physical mixture (LION+drug) was almost similar to that of the pure drug. The endothermic peak corresponding to the dehydration endotherm of MTX slightly shifted to  $\pm 3^\circ\text{C}$ . DSC thermograms demonstrate the absence of characteristic peaks of MTX in formulations confirming encapsulation of drug (MTX) in the nanoparticles (**Figure 5**).

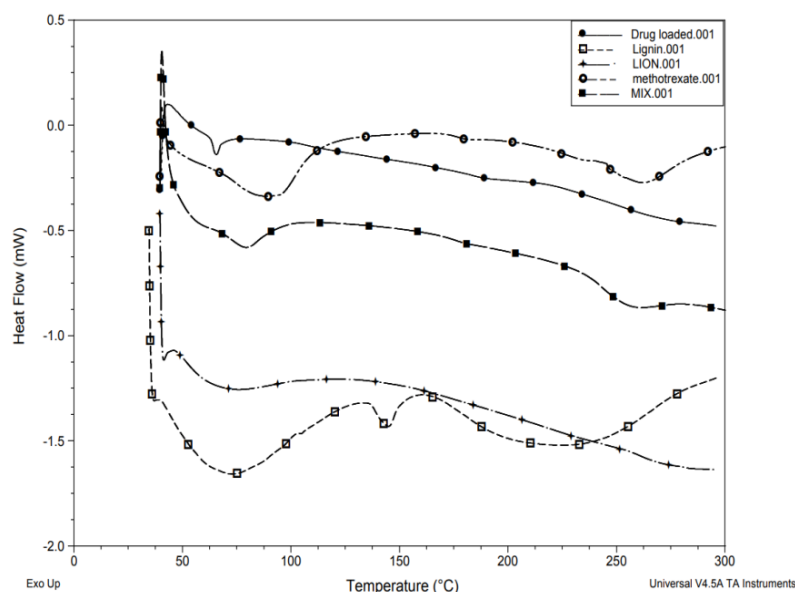


**Figure 5. DSC thermogram of drug-loaded nanoparticles, lignin, LION, drug (methotrexate), and physical mixture (MIX)**

#### **pH value and magnetic study:**

The pH of a formulation governs its pharmacokinetics, solubility, and even stability. The pH of blank and drug-loaded formulation (1% w/v, 25°C) was  $7.8 \pm 0.08$  and  $7.2 \pm 0.12$ , respectively. Blank (**Figure 6a**) and drug-loaded (**Figure 6b**) formulations when placed in an external magnetic field were attracted towards the magnet indicating the retention of the magnetic property of iron oxide. After removal of the magnetic field, particles were able to redisperse without any residual magnetization. Thus, the loading of the drug retained the magnetic property. Thereby, affirming the potential of the developed formulation as a delivery vehicle for specific targeted delivery in the body that upon exposure to an external magnetic field can be used for hyperthermia in cancer therapy and could also serve as a contrast agent in cancer imaging.



**a**



**b**

**Figure 6. Solution in presence (right) and absence (left) of an external magnetic field a. Blank b. Drug-loaded formulation**

***In-vitro* drug release studies:**

To evaluate the release profile of the formulation, the drug release study was measured at two different pH conditions i.e. 7.4 and 6.3. Neutral pH (7.4) as of blood/plasma was chosen to mimic the physiological pH when administered intravenously while pH 6.3 was chosen to mimic the tumor microenvironment.

The drug release followed the same pattern at both pHs but with slower release at pH 6.3. % Cumulative release of  $83.5 \pm 1.2\%$  and  $75.41 \pm 1.8\%$  occurred at 60 hours for pH 7.4 and 6.3, respectively with a maximum amount of drug released within 24 hours followed by slow sustained release (**Figure 7a**).

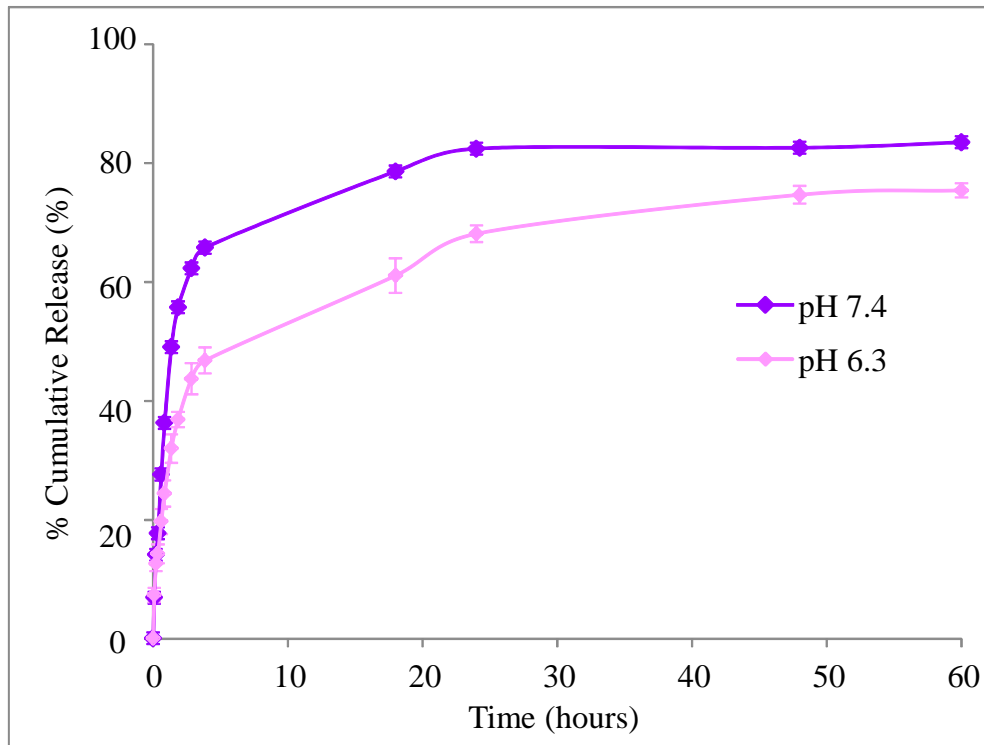


**Figure 7a. Drug release profiles at pH 6.3 and 7.4** (Data represent mean  $\pm$  SD; n = 3)

### Kinetic modeling

Kinetic modeling was done to understand the release kinetics of the prepared formulation by applying different equations to the obtained data sets of drug release. Various models were evaluated and the best fit model was selected with  $R^2$  (square of regression coefficient, R) and  $R^2$  adjusted closest to unity i.e. Weibull\_4 model.

The release kinetics followed by Weibull model is given by the equation below:

$$F = F_{\max} * [1 - e^{-(t-T_i)^{\beta}/\alpha}]$$

Where, F is the fraction of drug dissolved in time t,  $\alpha$  is a scale parameter that describes the time scale of the process,  $T_i$  represents the lag time before onset of dissolution. The term  $\beta$ , is a shape parameter that describes the shape of the curve as either exponential ( $\beta = 1$ ), sigmoid (S-shaped) with upward curvature followed by a turning point ( $\beta > 1$ ), or parabolic ( $\beta < 1$ ), with a higher initial slope and after that consistent with the exponential. The value of  $\beta \leq 0.75$  at both pH indicating a release that follows Fickian diffusion through fractal or euclidian spaces<sup>26</sup>, thus suggesting fickian release i.e. a concentration gradient dependent release

mechanism of the drug through the polymeric matrix. The expected and observed release is shown in Figure 7b.

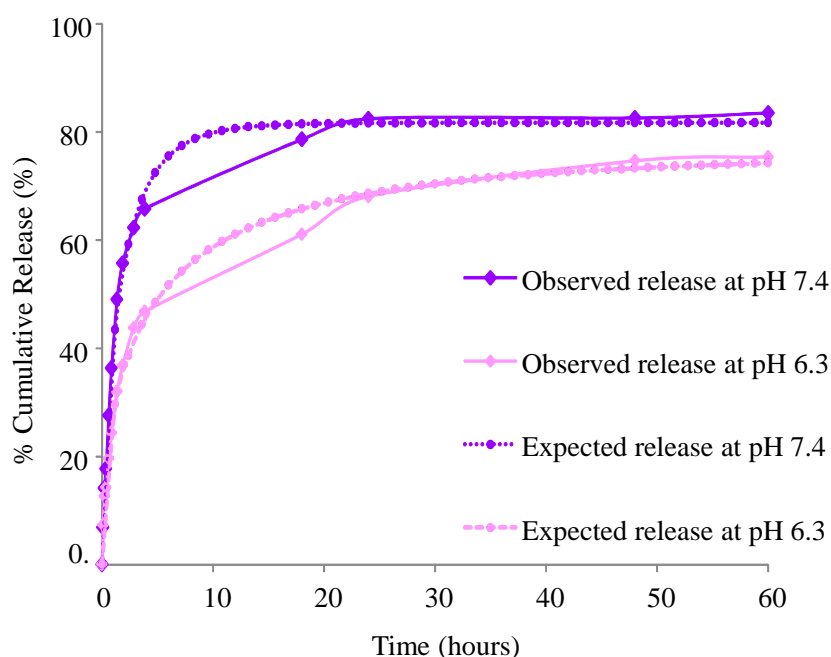


**Figure 7b. Expected & observed drug release profiles at pH 6.3 and 7.4**

### Stability studies

The stability of a formulation is critically important and therefore, particle size and polydispersity of lyophilized blank and drug-loaded nanoparticles was evaluated for a period of 12 months. The size was observed to be within the desired range with PDI values  $\geq 0.3$  in both blank and drug-loaded nanoparticles (**Figure 8**). To ensure uniform drug content, % drug loading was also measured of drug-loaded nanoparticles. The drug loading was observed to be uniform with  $66.06 \pm 0.18$ ,  $65.89 \pm 0.21$ , and  $65.57 \pm 0.23\%$  at 0, 6 and 12 months.

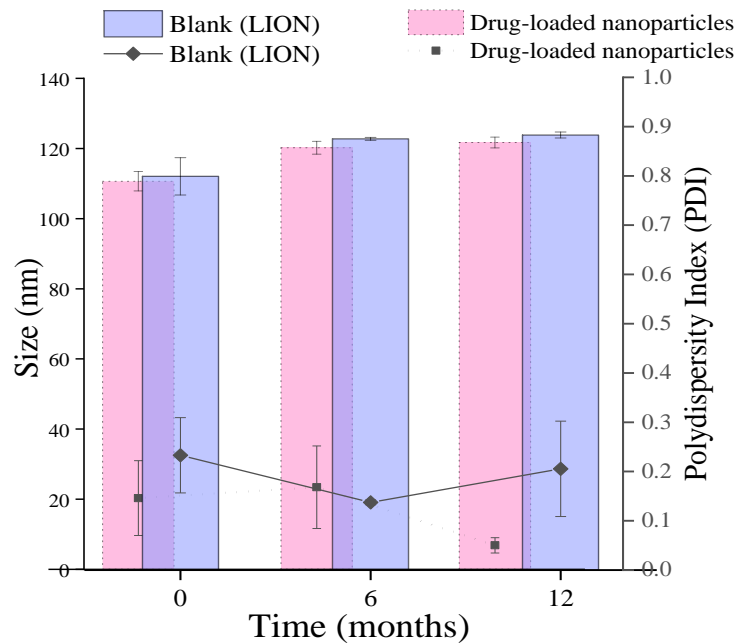


**Figure 8. Stability data of blank and drug-loaded nanoparticles**

### Antioxidant activity

The antioxidant property of lignin and iron oxide has been reported before and so, was analyzed using DPPH assay with ascorbic acid used as a positive control. A dose-dependent quenching of the DPPH free radicals was observed (**Figure 9**) with  $IC_{50}$  in the order: ascorbic acid ( $165.3 \pm 13.8 \mu\text{g/mL}$ ) > blank ( $739.2 \pm 43.5 \mu\text{g/mL}$ ) > drug-loaded nanoparticles ( $921.55 \pm 125.45 \mu\text{g/mL}$ ) > methotrexate ( $46.6 \text{ g/mL}$ ). Blank and drug-loaded nanoparticles showed good antioxidant property that can be attributed to the presence of polyphenolic groups in lignin and the neutralization of DPPH free-radical by electron transfer by iron oxide<sup>17</sup>. The antioxidant property of the formulation can be used to ameliorate the side effects and organ toxicity caused by methotrexate<sup>27</sup>.

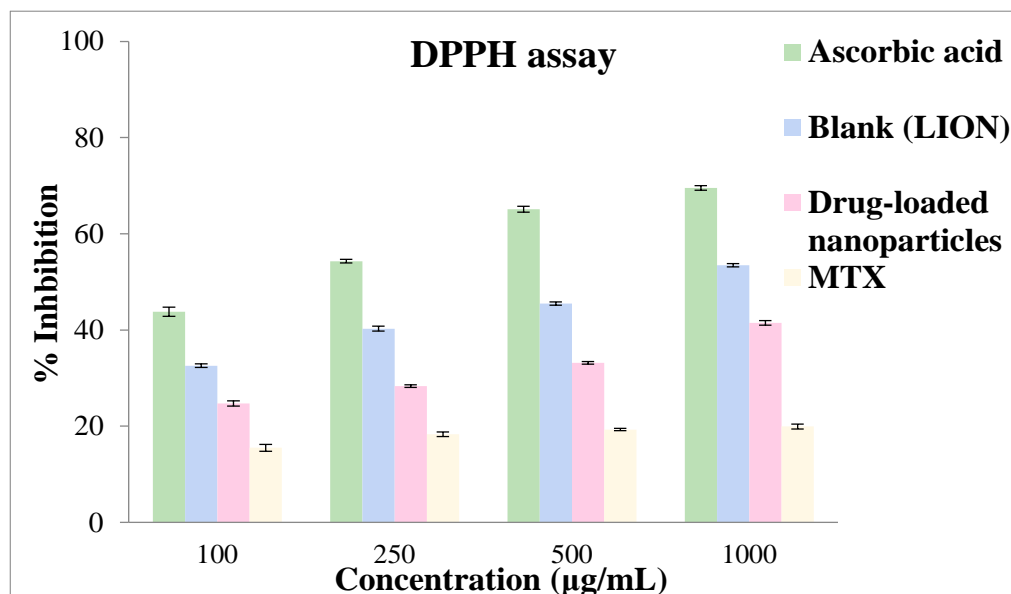




**Figure 9. DPPH assay at different concentrations of ascorbic acid, blank, drug-loaded nanoparticles, and methotrexate.**

Data represented as mean  $\pm$  SD; n = 3, Statistical analysis was performed using GraphPad Prism, ANOVA test. All values were significant ( $p < 0.01$ ) when compared with standard (ascorbic acid).

**Hemotoxicity**

Formulations administered through i.v. route should be compatible with the components of blood and so, hemotoxicity of blank, drug-loaded, and drug was measured at various concentrations (**Figure 10**). Any hemolysis value  $< 10\%$  is considered to be non-hemolytic while a value  $> 25\%$  hemolysis is considered to be hemolytic<sup>28</sup>. At the highest concentration (1000  $\mu\text{g/mL}$ ), the % hemolysis was  $3.67 \pm 0.0087$ ,  $5.97 \pm 0.0096$ , and  $6.3 \pm 0.0254\%$  for blank, drug-loaded, and drug solutions, respectively. These results indicate that the formulation is safe for administration.

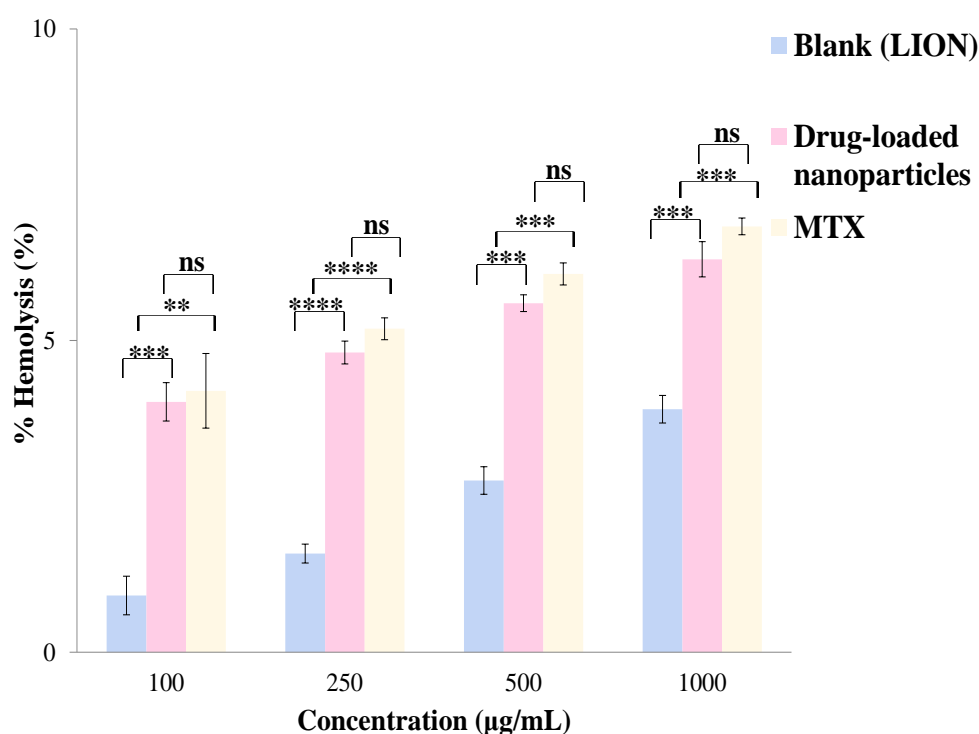


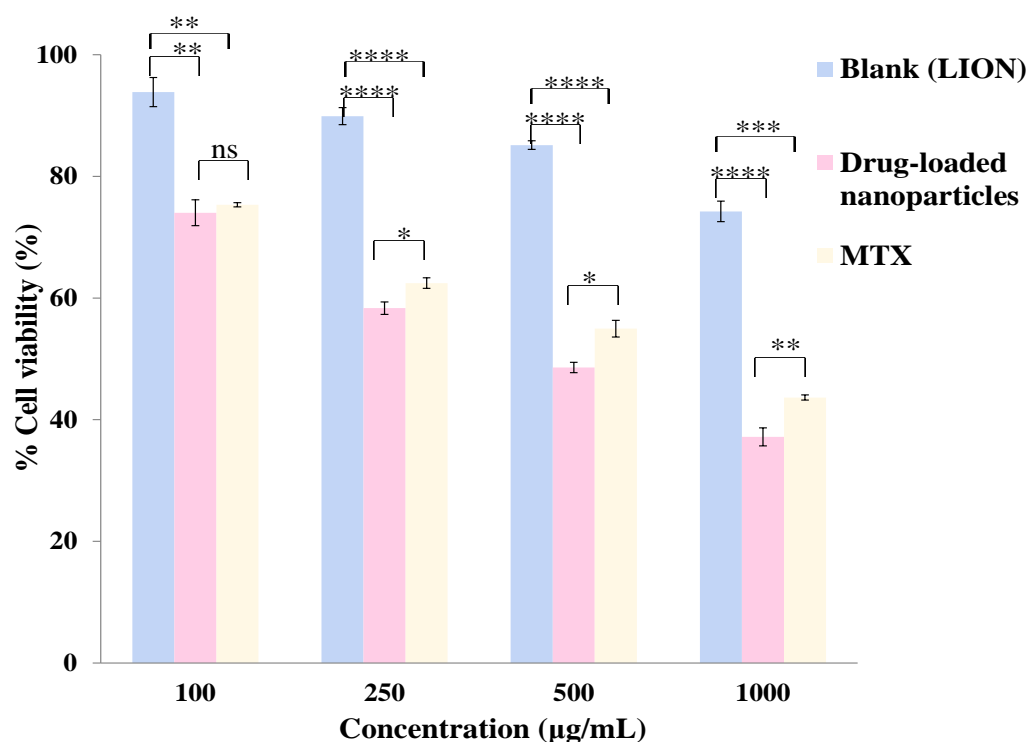
**Figure 10. Hemolytic assay at different concentrations of blank, drug-loaded nanoparticles, and MTX.**

Data represented as mean  $\pm$  SD; n = 3, Statistical analysis was performed using GraphPad Prism, ANOVA followed by Tukey's multiple comparison test. Significance was assigned at  $**p < 0.01$ ,  $***p < 0.001$ ,  $****p < 0.0001$ , and ns-non-significant.

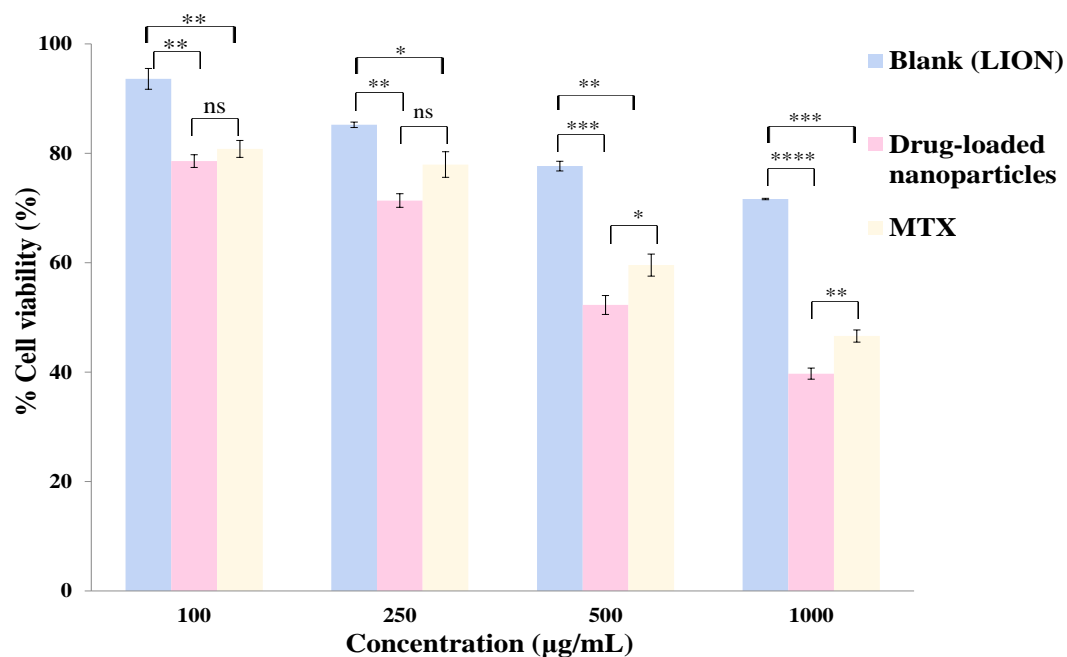
***In-vitro* cell-based studies:**

**Cytotoxicity**

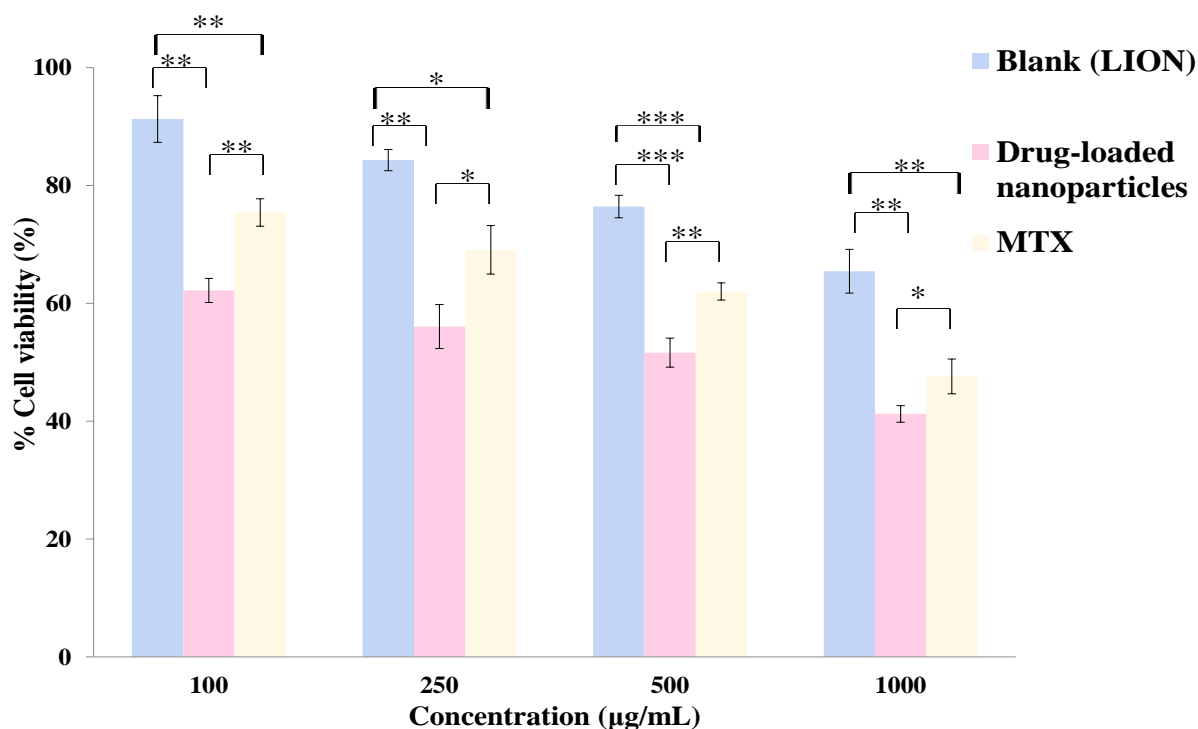
The potential of the formulation to cause cellular toxicity was evaluated using MTT assay. Different concentrations of LIONs, drug-loaded nanoparticles, and drug alone were evaluated for their cell viability against RAW, HeLa, and MDA-MB-231 cell lines (**Figures 11**). All the values were significant ( $p < 0.001$ ) when compared with control. The results showed significant cytotoxicity at the highest concentration (1000  $\mu\text{g/mL}$ ) for all the samples. The cytotoxic action of blank nanoparticles at high concentrations could be attributed to the presence of iron oxide. Iron oxide nanoparticles have been reported previously to cause cellular damage and death by causing oxidative stress by increased ROS production (by Fenton reaction, a redox reaction process catalyzed by  $\text{Fe}^{2+}/\text{Fe}^{3+}$  ions)<sup>29</sup>, inducing mitochondrial membrane potential collapse and mitochondrial swelling, cytochrome C release<sup>30</sup> and affecting cell homeostasis. The  $\text{IC}_{50}$  values are given in **Table 3**. The higher toxicity with formulation than drug alone shows synergistic action of iron-oxide and drug that could be further utilized for dose reduction and, in turn, alleviate the side effects and toxicity related with methotrexate administration.



a.



b.



c.

**Figure 11. Cytotoxicity assay at different concentrations of blank, drug-loaded nanoparticles, and MTX against a. RAW cell line b. HeLa cell line c. MDA-MB-231 cell line**

Data represented as mean  $\pm$  SD; n = 3, Statistical analysis was performed using GraphPad Prism, ANOVA followed by Tukey's multiple comparison test. Significance was assigned at \*p<0.05, \*\*p<0.01, \*\*\*p<0.001, \*\*\*\*p<0.0001, and ns-non-significant.

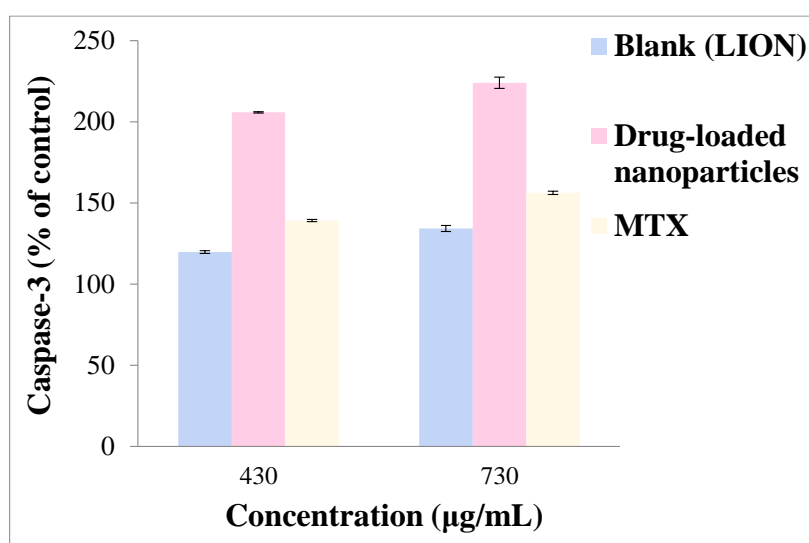
**Table 3.** IC<sub>50</sub> values in different cell lines

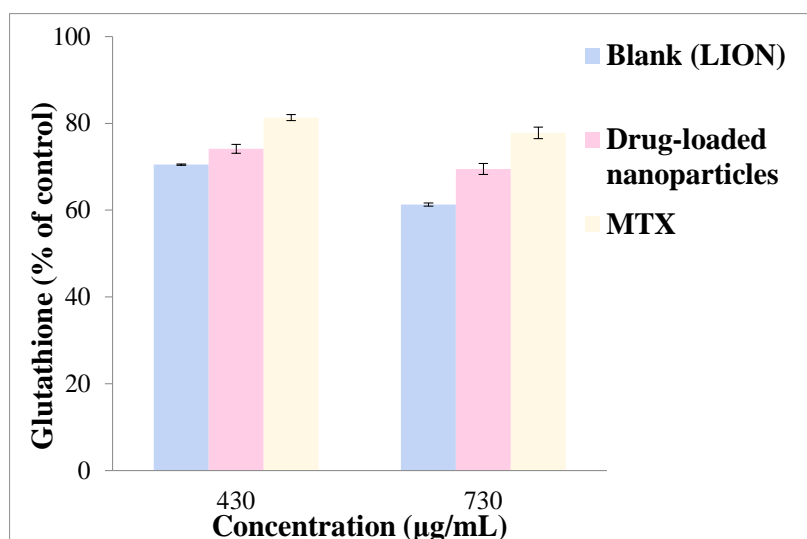
Cell line	IC <sub>50</sub> (ug/mL)		
	Blank (LION)	Drug-loaded nanoparticles	MTX
Raw	2789.5±321.5	434.05±81.25	565.2±131.2
HeLa	2113±342	578.6±73.6	789.65±121.45
MDA-MB-231	1711±219	431.9±147.5	733.35±166.55

**Caspase-3 and glutathione activity:**

Caspase-3, an important marker of apoptosis, was induced following treatment with blank, drug-loaded nanoparticles and MTX for 24 hours as shown in **Figure 12a**. Caspase-3 levels increased in a concentration-dependent manner in all three treatments. Compared to the control group, higher levels were seen after treatment with blank nanoparticles containing iron oxide and lignin, as reported previously<sup>31</sup>. The caspase-3 levels were higher in drug-loaded nanoparticles than MTX alone, suggesting a synergistic action of blank and drug nanoparticles as observed in the cytotoxicity studies.

GSH is one of the most important regulators of intracellular redox balance, performing an antioxidant cell-protective action, cycling between its reduced (GSH) and oxidized forms (GSSG). ROS-mediated apoptotic signaling is associated with a decrease in cellular GSH levels and loss of cellular redox balance and high levels of GSH have been associated with drug resistance<sup>32</sup>. Iron oxide nanoparticles have been previously reported to cause oxidative stress and reduce GSH levels which are influenced by the size and oxidation state of iron<sup>31</sup>. Iron oxide nanoparticle-induced oxidative stress was evident by drastic depletion of GSH levels on treatment with blank nanoparticles. As shown in **Figure 12b**, the reduction in drug-loaded nanoparticles was higher than with MTX. It has been demonstrated that GSH plays a possible role in MTX-induced apoptosis by contributing to maintaining cytochrome c in its reduced state under physiological conditions and preventing its apoptotic effect. Therefore, GSH depletion would favor cytochrome c-induced apoptosis by MTX<sup>32</sup>. The reduction in GSH levels by iron oxide nanoparticles could potentiate the action of MTX by inducing apoptosis mediated by cytochrome c release asserting the synergistic cytotoxicity of drug-loaded nanoparticles.

**a.**



b.

**Figure 12. *In-vitro* assay at different concentrations of blank, drug-loaded nanoparticles, and MTX of a. Caspase-3 and b. Glutathione in breast cancer cells**

Data represented as mean  $\pm$  SD; n = 3, Statistical analysis was performed using GraphPad Prism, ANOVA followed by Tukey's multiple comparison test. All values were significant with  $p < 0.001$ .

### Cellular uptake

The cellular uptake of FITC-labeled nanoparticles was analyzed using confocal fluorescence imaging. For imaging, nuclei of cells were stained with Hoechst 33342 (blue). The fluorescence images confirmed the internalization of FITC-labeled nanoparticles within 4 hours in breast carcinoma cell line (**Figure 13**). Importantly, it can be seen that the fluorescence intensity of drug-loaded nanoparticles was stronger than blank nanoparticles which can be attributed to the greater receptors-mediated endocytosis of methotrexate loaded nanoparticles. Thus, it indicates that the developed blank system could be used as a vehicle for drug delivery, especially for poorly water-soluble drugs like methotrexate.

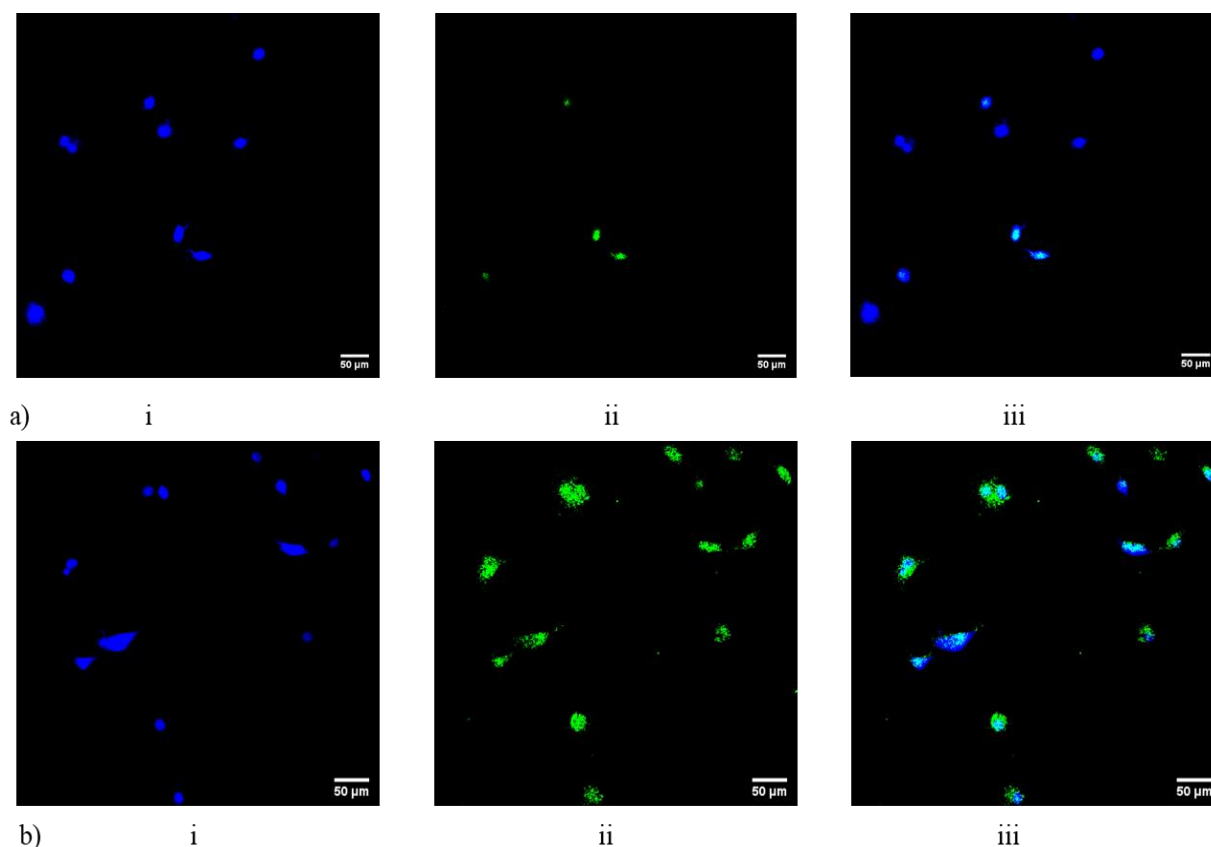


**Figure 13.** Confocal microscopy images of MDA-MB-231 cells incubated with a) FITC-labeled-blank and b) FITC-labeled-drug-loaded nanoparticles for 4h; (i), (ii), and (iii) represent Hoechst fluorescence (blue) FITC fluorescence (green) and merged fluorescence of Hoechst and FITC, respectively. (Scale bar=50um)

#### **Nuclear condensation and DNA fragmentation**

The MDA-MB-231 cells were treated with 1mg/mL doses of drug-loaded nanoparticles and MTX for 24 hours. Cells were stained with Hoechst 33342 DNA binds to adenine-thymine-rich regions of DNA and stain the minor groove. The shape of untreated cells showed normal morphology with majorly spindle and some round-shaped cells and formed a complete sheet with 60-70% confluency (**Figure 14a**). The cells incubated with drug-loaded nanoparticles and MTX (**Figure 14b and 14c**) showed decreased growth and apoptotic features like cellular rounding, and shrinkage, along with nuclear condensation and DNA fragmentation, indicated by arrow. The observed cellular damage was slightly higher in drug-loaded nanoparticles than in the drug alone, thus suggesting the synergistic action of iron oxide, lignin, and methotrexate, as observed in cytotoxicity studies.

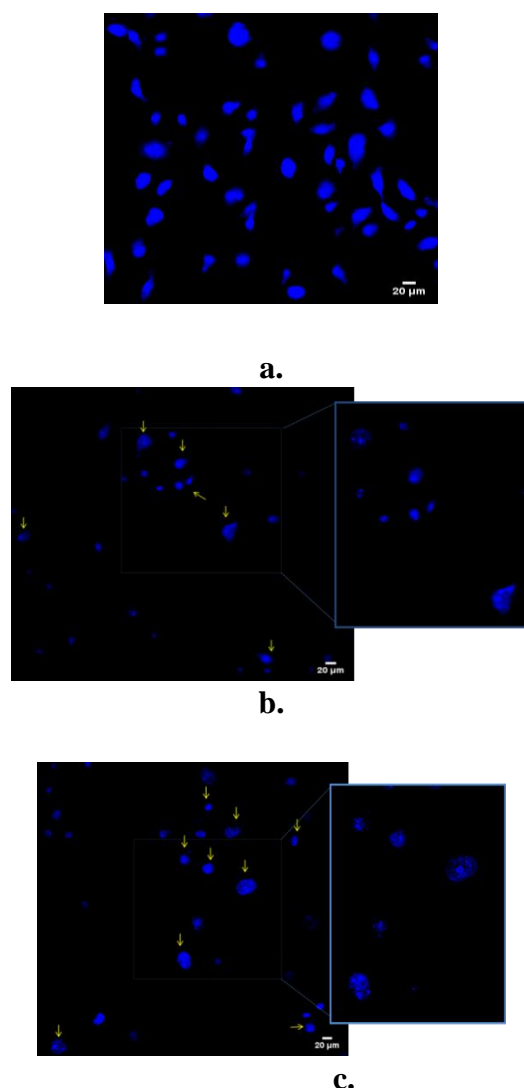


**Figure 17. Confocal microscopy images of MDA-MB-231 cells stained with Hoechst dye**  
**a. without treatment (control); after treatment with b. drug-loaded nanoparticles**  
**(formulation) and c. MTX (arrow represents DNA fragmentation)**

### **Statistical Analysis**

All experiments were performed in triplicate. All data presented hereinafter is reported as the mean  $\pm$  standard deviation (SD). A p-value of less than 0.05 was considered to be statistically significant. Statistical analysis was performed using the GraphPad Prism using ANOVA followed by Tukey's multiple comparison test. \* $p < 0.05$ , \*\* $p < 0.01$  \*\*\* $p < 0.001$ , and \*\*\*\* $p < 0.0001$ .

### **Conclusion**

The nanoparticles were prepared using different methods and the successful synthesis was done using three sequential techniques i.e., chemical co-precipitation, anti-solvent, and ultrasonication method. The prepared nanoparticles were optimized by varying the drug: polymer ratio and evaluated for their physicochemical characteristics. Spherical nanoparticles with a non-uniform surface and narrow size range of 110-130 nm were confirmed with DLS,

HRTEM, and FESEM analysis. The nanoparticles were in the optimal size range for passive targeting via EPR effect on tumor tissue and the same hand successfully evades clearance by renal, liver, and reticuloendothelial systems. Qualitative analysis by FT-IR and DSC confirmed the effective encapsulation of the drug and formation of the nano-hybrid. The polymeric coating of lignin effectively increased the stability of iron oxide.

The delivery of the drug to the cancer site was aimed at exploiting the magnetic characteristic of iron oxide which was analyzed by placing the prepared formulation in an external magnetic field that confirmed that the drug-loaded nanoparticles retained the magnetic property of iron oxide even after polymeric coating. The pH of the formulation was near neutral (~7.2).

The optimized polymer:drug (1:3) ratio with maximum drug loading (65%) and encapsulation efficiency (66%) was evaluated for its *in-vitro* release characteristic which showed Weibull\_4 order release kinetics with fickian release profile. The release was slower at slightly acidic pH (pH 6.3) with nearly 82% and 68% release in 24 hours at pH 7 and 6.3, respectively, followed by slow sustained release. *In vitro* hemolytic assay assured the biocompatibility of the prepared carrier system and *ex-vivo* radical scavenging activity showed its antioxidant potential. The cytotoxic evaluation demonstrated an efficient dose-dependent cytotoxicity towards breast cancer, cervical cancer and murine macrophage cell lines with synergistic cytotoxic action of iron oxide, lignin, and methotrexate. The cellular uptake of drug-loaded nanoparticles was visibly higher confirming the receptor-mediated endocytosis of methotrexate-loaded nanoparticles. The formulation showed DNA damage along with nuclear condensation and induction of apoptosis by activation of caspase-3 and oxidative stress in breast cancer cell line. Overall, the developed lignin-based drug delivery system showed suitable characteristics and with further research can prove to be a promising tool for chemotherapeutics.

### **Impact of the research in the advancement of knowledge or benefit to mankind**

This study reports a new method of synthesis for methotrexate-loaded lignin-iron oxide nanoparticles for use in cancer therapy. The nanoparticles obtained were smooth and of optimal size required for chemotherapy. Despite centuries of research, cancer remains a debilitating disease impacting not only the patient but also the caregiver. A multitude of adversities ranging from physical health to emotional well-being. The patient experiences nausea, pain, vomiting, hair loss, weakened immune system, fear anxiety, depression, stigma and emotional distress. This research aims to design novel approach of methotrexate along with magnetic therapy to enhance anticancer activity therein reducing drug dose and side effects.

Lignin is a natural phenolic polymer with abundant advantages such as antioxidant, anti-inflammatory, anticancer activities but is still unexplored for its polymeric potential in formulation design and development. In this research study we aim to study the potential of lignin in drug loading and chemotherapy. Additionally, this research explores the efficacy of magnetic nanoparticles in combination with chemotherapy in cancer treatment. The studies show promising results and suggests the superiority of nanoparticle-based combination treatment of magnetic nanoparticles and chemotherapy in treatment of cancer and also sheds light on cellular aspect of the therapy. The study also reports synergistic anticancer activity observed with lignin, iron-oxide, and methotrexate.



## Literature references

1. Sung, H. *et al.* Global Cancer Statistics 2020: GLOBOCAN Estimates of Incidence and Mortality Worldwide for 36 Cancers in 185 Countries. *CA. Cancer J. Clin.* **71**, 209–249 (2021).
2. Senapati, S., Mahanta, A. K., Kumar, S. & Maiti, P. Controlled drug delivery vehicles for cancer treatment and their performance. *Signal Transduct. Target. Ther.* **3**, 1–19 (2018).
3. Chenthamara, D. *et al.* Therapeutic efficacy of nanoparticles and routes of administration. *Biomater. Res.* **23**, 1–29 (2019).
4. Fang, J., Nakamura, H. & Maeda, H. The EPR effect: Unique features of tumor blood vessels for drug delivery, factors involved, and limitations and augmentation of the effect. *Adv. Drug Deliv. Rev.* **63**, 136–151 (2011).
5. Shi, Y., van der Meel, R., Chen, X. & Lammers, T. The EPR effect and beyond: Strategies to improve tumor targeting and cancer nanomedicine treatment efficacy. *Theranostics* **10**, 7921–7924 (2020).
6. Peer, D. *et al.* 84 Nat nanotech 2007 R Langer Nanocarriers as an emerging platform for cancer therapy.pdf. *Nat. Nanotechnol.* **2**, 751–760 (2007).
7. Wei, Q. Y., Xu, Y. M. & Lau, A. T. Y. Recent progress of nanocarrier-based therapy for solid malignancies. *Cancers (Basel)*. **12**, 1–37 (2020).
8. NDong, C. *et al.* Tumor cell targeting by iron oxide nanoparticles is dominated by different factors in vitro versus in vivo. *PLoS One* **10**, 1–18 (2015).
9. Vakili-Ghartavol, R. *et al.* Toxicity assessment of superparamagnetic iron oxide nanoparticles in different tissues. *Artif. Cells, Nanomedicine Biotechnol.* **48**, 443–451 (2020).
10. Osaci, M. & Cacciola, M. Influence of the magnetic nanoparticle coating on the magnetic relaxation time. *Beilstein J. Nanotechnol.* **11**, 1207–1216 (2020).
11. Capecchi, E. *et al.* Functionalized tyrosinase-lignin nanoparticles as sustainable catalysts for the oxidation of phenols. *Nanomaterials* **8**, (2018).
12. Thakur, V. K. & Thakur, M. K. Recent advances in green hydrogels from lignin: A review. *Int. J. Biol. Macromol.* **72**, 834–847 (2015).
13. Raj Giri, B. *et al.* Improved Bioavailability and High Photostability of Methotrexate by Spray-Dried Surface-Attached Solid Dispersion with an Aqueous Medium. *Pharmaceutics* **13**, 111 (2021).
14. Ma, Y. zhi, Zheng, D. feng, Mo, Z. ye, Dong, R. jing & Qiu, X. qing. Magnetic lignin-based carbon nanoparticles and the adsorption for removal of methyl orange. *Colloids Surfaces A Physicochem. Eng. Asp.* **559**, 226–234 (2018).
15. Dai, L., Liu, R., Hu, L. Q., Zou, Z. F. & Si, C. L. Lignin Nanoparticle as a Novel Green Carrier for the Efficient Delivery of Resveratrol. *ACS Sustain. Chem. Eng.* **5**, 8241–8249 (2017).
16. Liu, Z. & Yang, L. Antisolvent precipitation for the preparation of high polymeric procyanidin nanoparticles under ultrasonication and evaluation of their antioxidant activity in vitro. *Ultrason. Sonochem.* **43**, 208–218 (2018).

17. Sandhya, J. & Kalaiselvam, S. Biogenic synthesis of magnetic iron oxide nanoparticles using inedible borassus flabellifer seed coat: Characterization, antimicrobial, antioxidant activity and in vitro cytotoxicity analysis. *Mater. Res. Express* **7**, (2020).
18. Muga, J. O., Gathirwa, J. W., Tukulula, M. & Jura, W. G. Z. O. In vitro evaluation of chloroquine-loaded and heparin surface-functionalized solid lipid nanoparticles. *Malar. J.* **17**, 1–7 (2018).
19. Carissimi, G., Montalbán, M. G., Vllora, G. & Barth, A. Direct quantification of drug loading content in polymeric nanoparticles by infrared spectroscopy. *Pharmaceutics* **12**, 1–15 (2020).
20. Alqahtani, M. S., Alqahtani, A., Al-Thabit, A., Roni, M. & Syed, R. Novel lignin nanoparticles for oral drug delivery. *J. Mater. Chem. B* **7**, 4461–4473 (2019).
21. Moghtaderi, H., Sepehri, H., Delphi, L. & Attari, F. Gallic acid and curcumin induce cytotoxicity and apoptosis in human breast cancer cell MDA-MB-231. *BioImpacts* **8**, 185–194 (2018).
22. Wu, C. W. *et al.* Combined treatment with Vitamin C and methotrexate inhibits triple-negative breast cancer cell growth by increasing H<sub>2</sub>O<sub>2</sub> accumulation and activating caspase-3 and p38 pathways. *Oncol. Rep.* **37**, 2177–2184 (2017).
23. Ganguly, M. & Pramanik, D. Pectin coated iron oxide nanocomposite - A vehicle for controlled release of curcumin. *Int. J. Biol. Biomed. Eng.* **11**, 143–160 (2017).
24. Klapiszewski, Ł. *et al.* Magnetite nanoparticles conjugated with lignin: A physicochemical and magnetic study. *Appl. Surf. Sci.* **422**, 94–103 (2017).
25. Fuliş, A. *et al.* Thermoanalytical and spectroscopic study on methotrexate - active substance and tablet. *Dig. J. Nanomater. Biostructures* **9**, 93–98 (2014).
26. Papadopoulou, V., Kosmidis, K., Vlachou, M. & Macheras, P. On the use of the Weibull function for the discernment of drug release mechanisms. *Int. J. Pharm.* **309**, 44–50 (2006).
27. Vardi, N., Parlakpınar, H., Cetin, A., Erdogan, A. & Ozturk, I. C. Protective effect of  $\beta$ -carotene on methotrexate-induced oxidative liver damage. *Toxicol. Pathol.* **38**, 592–597 (2010).
28. Psimadas, D., Georgoulis, P., Valotassiou, V. & Loudos, G. Molecular Nanomedicine Towards Cancer : *J. Pharm. Sci.* **101**, 2271–2280 (2012).
29. Laqué-Rupérez, E., Ruiz-Gómez, M. J., De La Peña, L., Gil, L. & Martínez-Morillo, M. Methotrexate cytotoxicity on MCF-7 breast cancer cells is not altered by exposure to 25 Hz, 1.5 mT magnetic field and iron (III) chloride hexahydrate. *Bioelectrochemistry* **60**, 81–86 (2003).
30. Jahanbani, J. *et al.* Selective anticancer activity of superparamagnetic iron oxide nanoparticles (SPIONs) against oral tongue cancer using in vitro methods: The key role of oxidative stress on cancerous mitochondria. *J. Biochem. Mol. Toxicol.* **34**, 1–8 (2020).
31. Yarjanli, Z., Ghaedi, K., Esmaeili, A., Rahgozar, S. & Zarrabi, A. Iron oxide nanoparticles may damage to the neural tissue through iron accumulation, oxidative stress, and protein aggregation. *BMC Neurosci.* **18**, 1–12 (2017).
32. Barros, S. *et al.* The Redox State of Cytochrome C Modulates Resistance to Methotrexate in Human MCF7 Breast Cancer Cells. *PLoS One* **8**, 1–12 (2013).